Computer Physics Communications 267 (2021) 108061

Contents lists available at ScienceDirect

Computer Physics Communications

www.elsevier.com/locate/cpc

São Paulo potential version 2 (SPP2) and Brazilian nuclear potential (BNP) ☆,☆☆

L.C. Chamon [a,*], B.V. Carlson [b], L.R. Gasques [a]

[a] Universidade de Sao Paulo, Instituto de Fisica, Rua do Matao, 1371, 05508-090, Sao Paulo, SP, Brazil
[b] Departamento de Física, Instituto Tecnológico de Aeronáutica, Centro Técnico Aeroespacial, São José dos Campos, SP, Brazil

ARTICLE INFO

Article history:
Received 26 December 2020
Received in revised form 15 March 2021
Accepted 20 May 2021
Available online 11 June 2021

Keywords:
Nuclear density
Nuclear interaction
Optical potential

ABSTRACT

The REGINA code calculates the São Paulo potential version 2 (SPP2) and the Brazilian nuclear potential (BNP). The code also provides nuclear densities obtained from the Dirac-Hartree-Bogoliubov model, which are used to calculate the nuclear potentials. Elastic scattering cross sections are obtained within the context of the optical model, with different options for the real and imaginary parts of the optical potential. In this manuscript, we provide a summary of the theoretical framework and information about the use of the code.

Program summary

Program Title: REGINA.f
CPC Library link to program files: https://doi.org/10.17632/vfkkjb8dv7.1
Licensing provisions: GPLv3
Programming language: Fortran-77
Nature of problem: We provide a code to calculate the nuclear potential between two nuclei according to two different models: the São Paulo potential version 2 (SPP2), that includes a dependence on the relative velocity between the nuclei, and the velocity independent Brazilian nuclear potential (BNP). These potentials assume the effective nuclear interactions proposed in [1,2], and are obtained within the double-folding approach with nuclear densities calculated through the Dirac-Hartree-Bogoliubov model [3].
Solution method: The code involves two files containing previously calculated results for theoretical neutron and proton distributions and also experimental charge densities obtained from electron scattering experiments. These results are used to obtain matter densities through convolution using Fourier transforms. The Fourier transform method is also employed to obtain the double-folding potentials. Integration of the Schrödinger equation with a complex optical potential is performed using the Cowell method [4,5]. With this, for a given system and energy, we obtain the S-matrix and the elastic scattering cross sections.
Additional comments including restrictions and unusual features: The maximum angular momentum supported in the optical model calculations is 2000.

1. Introduction

In this paper, we present two theoretical models for the mean field nuclear interaction between two nuclei and provide a code to calculate these potentials. The models are based on the double-folding method, and differ with regard to the effective nuclear interaction assumed in the calculations. The code involves two files: one containing nuclear distributions obtained through the theoretical Dirac-Hartree-Bogoliubov (DHB) model [3], and another with experimental charge densities obtained from electron scattering experiments. With these, neither interaction has adjustable parameters and, therefore, both can be used to obtain standard predictions in nuclear reactions. In particular, one of the models can be considered as an improvement of the São Paulo potential (SPP) [6], which has been widely employed in nuclear reactions data analyses (to date, [6] has more than 400 citations). We name the present theoretical models as the São Paulo potential version 2

☆ The review of this paper was arranged by Prof. Z. Was.
☆☆ This paper and its associated computer program are available via the Computer Physics Communications homepage on ScienceDirect (http://www.sciencedirect.com/science/journal/00104655).

* Corresponding author.
E-mail address: lchamon@if.usp.br (L.C. Chamon).

https://doi.org/10.1016/j.cpc.2021.108061
0010-4655/

(SPP2) and the Brazilian nuclear potential (BNP). The code also allows the calculation of elastic scattering cross sections within the context of the optical model (OM). The SPP2 or BNP can be assumed for the real part of the optical potential (OP), while the user can choose different values for several parameters that result in different shapes and strengths for its imaginary part.

2. The nuclear densities and the double-folding potential

Several models for double-folding potentials are associated with the nucleon distributions of the nucleus, which are often also called matter densities. However, within the context of the SPP and BNP models, matter densities and nucleon distributions have different meanings. Thus, we provide below the definitions of densities and distributions.

For a given nucleus, the corresponding proton distribution at a certain radius multiplied by the volume element, $\rho_p(\vec{r}) \times d\vec{r}$, provides the probability to find one proton inside that volume. A similar definition is related to the neutron distribution $\rho_n(\vec{r})$. The nucleon distribution of the nucleus corresponds to the sum of the proton and neutron ones: $\rho_N(\vec{r}) = \rho_p(\vec{r}) + \rho_n(\vec{r})$. Thus, the multiplication of $\rho_N(\vec{r})$ by $d\vec{r}$ provides the probability to find one nucleon inside that volume. The nucleon distribution is normalized as:

$$\int \rho_N(\vec{r})\, d\vec{r} = Z + N = A. \tag{1}$$

For the same nucleus, the corresponding charge density at a certain radius multiplied by the volume element, $\rho_c(\vec{r}) \times d\vec{r}$, provides the amount of charge inside that volume. The charge density is normalized as:

$$\int \rho_c(\vec{r})\, d\vec{r} = Z. \tag{2}$$

The proton itself has an intrinsic charge density, for which we assume the notation: $\rho_{c/p}$ (we do not associate a charge density to the neutron). Therefore, the charge density of the nucleus can be obtained through a folding of the corresponding proton distribution of the nucleus with the intrinsic charge density of one proton:

$$\rho_c(\vec{r}) = \int \rho_p(\vec{r})\, \rho_{c/p}(\vec{r'} - \vec{r})\, d\vec{r'}. \tag{3}$$

Now we define the intrinsic matter density of one nucleon (proton or neutron) and assume that it is equal the intrinsic charge density of one proton: $\rho_{m/N}(\vec{r}) = \rho_{c/p}(\vec{r})$. In addition, in analogy with Eq. (3), we define the matter density of a nucleus through a folding of the corresponding nucleon distribution of the nucleus with the intrinsic matter density of one nucleon:

$$\rho_m(\vec{r}) = \int \rho_N(\vec{r})\, \rho_{m/N}(\vec{r'} - \vec{r})\, d\vec{r'}. \tag{4}$$

The matter density of a nucleus is thus normalized as:

$$\int \rho_m(\vec{r})\, d\vec{r} = A. \tag{5}$$

The charge densities of the nuclei can be related to the Coulomb potential, by considering the electrostatic interaction between two elements of charge of the nuclei, $dq_1 = e\, \rho_{c1}(\vec{r}_1)\, d\vec{r}_1$ and $dq_2 = e\, \rho_{c2}(\vec{r}_2)\, d\vec{r}_2$. This fundamental interaction is given by: $v_{qq}(r_{12}) = \frac{dq_1\, dq_2}{r_{12}}$, where r_{12} is the distance between the two elementary charges. With this, we obtain the Coulomb potential between two nuclei as:

$$\begin{aligned} V_C(\vec{R}) &= \int \frac{1}{|\vec{R} - \vec{r}_1 + \vec{r}_2|}\, dq_1\, dq_2 \\ &= \int \rho_{c1}(\vec{r}_1)\, \rho_{c2}(\vec{r}_2)\, \frac{e^2}{|\vec{R} - \vec{r}_1 + \vec{r}_2|}\, d\vec{r}_1\, d\vec{r}_2. \end{aligned} \tag{6}$$

In this equation, $\vec{r}_i$ represent the vector that connects the center of mass of nucleus i to the respective volume element, while $\vec{R}$ connects the centers of masses of the two nuclei.

Analogously, we obtain the nuclear potential between two nuclei by considering the nuclear interaction between two elements of matter of the nuclei, $v_{mm}(\vec{r}_{12})$, as:

$$\begin{aligned} V_N(\vec{R}) &= \int v_{mm}(\vec{R} - \vec{r}_1 + \vec{r}_2)\, dm_1\, dm_2 \\ &= \int \rho_{m1}(\vec{r}_1)\, \rho_{m2}(\vec{r}_2)\, v_{mm}(\vec{R} - \vec{r}_1 + \vec{r}_2)\, d\vec{r}_1\, d\vec{r}_2. \end{aligned} \tag{7}$$

The difference between the SPP and BNP is related to the model assumed for $v_{mm}(\vec{r}_{12})$.

Since the matter density is related to the nucleon distribution according to Eq. (4), Eq. (7) can be rewritten as:

$$V_N(\vec{R}) = \int \rho_{N1}(\vec{r}_1)\, \rho_{N2}(\vec{r}_2)\, v_{NN}(\vec{R} - \vec{r}_1 + \vec{r}_2)\, d\vec{r}_1\, d\vec{r}_2, \tag{8}$$

where we define the effective nucleon-nucleon interaction as:

$$v_{NN}(\vec{r}) = \int \rho_{m/N}(\vec{r}_1)\, \rho_{m/N}(\vec{r}_2)\, v_{mm}(\vec{r} - \vec{r}_1 + \vec{r}_2)\, d\vec{r}_1\, d\vec{r}_2. \tag{9}$$

Most models for the double-folding potential assume Eq. (8), with the nucleon distributions of the nuclei and the effective nucleon-nucleon interaction. The SPP and BNP are calculated assuming the alternative Eq. (7), with the matter densities of the nuclei and the effective nuclear interaction between two elements of matter. Note that both forms of calculating the folding potential are mathematically equivalent if we assume the definitions in Eqs. (4) and (9). On the other hand, Eq. (7) for the nuclear interaction provides an interesting analogy with Eq. (6) of the Coulomb potential.

3. The first version of the São Paulo potential

The first version of the SPP [6] has been successful in describing the elastic scattering (see e.g. [7,8]), peripheral reaction channels (see e.g. [9,10]) and fusion (see e.g. [11,12]) for several heavy-ion systems in a very wide energy region. Within this model, the nuclear interaction is connected with the folding potential through:

$$V_N(R) = V_F(R)\, e^{-4\mathrm{v}^2/c^2}, \tag{10}$$

where c is the speed of light and v is the local relative velocity between the two nuclei. The velocity is related to the kinetic energy,

$$E_K(R, E_{c.m.}) = E_{c.m.} - V_C(R) - V_N(R), \tag{11}$$

through the relativistic expression:

$$\mathrm{v}^2(R, E_{c.m.})/c^2 = 1 - \left(\frac{\mu c^2}{\mu c^2 + E_K}\right)^2. \tag{12}$$

V_C is the Coulomb potential and μ is the reduced rest mass of the system. Within the SPP, the folding potential depends on the matter densities of the nuclei involved in the collision as follows:

$$V_F(R) = \int \rho_{m1}(\vec{r}_1)\, \rho_{m2}(\vec{r}_2)\, V_0\, \delta(\vec{R} - \vec{r}_1 + \vec{r}_2)\, d\vec{r}_1\, d\vec{r}_2, \tag{13}$$

with $V_0 = -456$ MeV fm^3. The use of the δ function in Eq. (13) is called the zero-range approach.

An important characteristic of the SPP is the systematic for nuclear densities. In [6], we assumed a two-parameter Fermi function to describe the nuclear densities:

$$\rho(r) = \frac{\rho_0}{1 + \exp\left(\frac{r-R_0}{a}\right)}. \quad (14)$$

In that paper, we presented an extensive systematic for the densities of tightly-bound stable nuclei, based on theoretical calculations with the DHB model and also on experimental results for charge distributions (obtained from electron scattering). We found that the radii of the charge and matter densities on average can be represented by:

$$R_{0\,\mathrm{charge}} = 1.76Z^{1/3} - 0.96\,\mathrm{fm}, \quad (15)$$

$$R_{0\,\mathrm{matter}} = 1.31A^{1/3} - 0.84\,\mathrm{fm}. \quad (16)$$

The charge and matter distributions present average diffuseness values of $a = 0.53$ fm and $a = 0.56$ fm, respectively. Of course, small deviations around these average values are expected due to the effects of the structure of the nuclei.

Within the context of the systematic for the densities, the SPP has no adjustable parameter. An extension of the model for the imaginary part of the optical potential was proposed in [7]. It was found that, for many systems and energies, experimental angular distributions are well described by OM calculations, in which the SPP is assumed for the real part of the OP, while the imaginary part is assumed to be proportional to the SPP normalized by a factor of about 0.8. In this context, the SPP is a totally parameter-free model (real and imaginary parts of the OP). Due to these characteristics, the model has been widely used to obtain standard predictions in data analyses of elastic scattering and reaction channels.

The SPP has been used in the context of the systematic for the nuclear densities. However, effects of the structure of the nuclei are not included in the average R_0 and a values of this systematic. Furthermore, the study of nuclear reactions involving nuclei very far from the line of stability is currently very intense. Of course, the densities of these nuclei are quite different from those of the original systematic of the SPP. On the other hand, the lack of adjustable parameters of the SPP makes it a powerful tool to provide theoretical predictions and to be used as a comparative standard in data analyses. This is an important characteristic of the model. Thus, we have developed a second version of the model (SPP2) with the purpose of working with realistic densities, even for quite exotic nuclei, and keeping the predictive characteristic of the model.

Recently, several works [13–15] have demonstrated that the energy-dependence of the OP that describe elastic scattering data through OM calculations could in fact be related to effects of inelastic couplings to states of high excitation energies. In this approach, the nuclear interaction should be independent of energy. Thus, in the present paper we also provide the energy independent BNP to be used in coupled-channel calculations for heavy-ion systems.

4. The BNP and SPP2 effective nuclear interactions

Due to the lack of open reaction channels, the data analysis of $\alpha + \alpha$ elastic scattering at low energies through the OM must be performed without an imaginary part in the OP. This makes the theoretical cross sections very sensitive to the real part of the OP. Alternatively, the data fit can be performed adjusting phase-shifts. In this case, the phase-shifts should be real (no absorption), relative only to even angular momenta (identical particles), and involve just a few L values (low energy range). In these conditions, the values of phase-shifts have been obtained from data analyses with quite good accuracy.

In [16], we analyzed the $\alpha + \alpha$ phase-shifts at low energies in the context of the SPP. To account for the data, the strength of the SPP has to be increased by about 10%. Nevertheless, the renormalization factor presents a small but inconvenient angular momentum dependence.

In [1], we successfully proposed a new model to describe the low energy $\alpha + \alpha$ experimental phase-shifts within the context of the double-folding approach. The respective effective nuclear interaction has the following form:

$$v_{mm}(\vec{r}) = -U_0\, f(r). \quad (17)$$

Four trial shapes for $f(r)$ were tested and all of them provided similar and very good data fits. The four functions resulted in quite similar values for the volume integral and root-mean square radius of $v_{mm}(\vec{r})$: $V_0 \approx 417$ MeV fm^3 and $r_{RMS} \approx 1.2$ fm. Since the four trial functions provide similar $\alpha + \alpha$ data fits, we assume here the following one:

$$v_{mm}(\vec{r}) = -U_0\, e^{-(r/a)^2}, \quad (18)$$

with $U_0 = 87.226$ MeV and $a = 0.95$ fm. We call Eq. (18) the BNP effective nuclear interaction.

Equation (18) does not contain any dependence on the relative velocity. On the other hand, the dependence on the velocity is important in the context of the SPP to describe the elastic scattering at low and intermediate energy range within the same approach. Thus, in [2] we reanalyzed the $\alpha + \alpha$ phase-shift data set at low energies but now using the following interaction:

$$v_{mm}(\vec{r}) = -U_0\, f(r)\, e^{-4v^2/c^2}. \quad (19)$$

Again different trial functions provided similar data fits, but now the corresponding volume integrals and root-mean square radii result in: $V_0 \approx 512$ MeV fm^3 and $r_{RMS} \approx 0.60$ fm. We assume here the following interaction:

$$v_{mm}(\vec{r}) = -U_0\, e^{-(r/a)^2}\, e^{-4v^2/c^2}, \quad (20)$$

with $U_0 = 735.813$ MeV and $a = 0.50$ fm. We call Eq. (20) the SPP2 effective nuclear interaction.

Note that both effective BNP and SPP2 interactions were determined through phase-shift data fits for $\alpha + \alpha$ elastic scattering at low energies, since, in this case, due to the lack of open reaction channels, a null imaginary potential must be assumed in the OM calculations. The SPP2 interaction depends on the local relative velocity according to Eq. (20), while the velocity term is missing from the BNP, Eq. (18). Due to the lack of the OP imaginary part, the $\alpha + \alpha$ theoretical phase-shifts are quite sensitive to the real part, including the inner region of small R. Due to the local characteristics of the velocity-dependence (the velocity depends on R through Eqs. (11) and (12)), the BNP and SPP2 shapes of the real part of the OP (at a fixed bombarding energy) are different. Thus, even at the low energy region, the $\alpha + \alpha$ theoretical phase-shifts are sensitive to the velocity-dependence, and the parameter values of Eqs. (18) and (20) could be accurately determined. In principle, even closed reaction channels could affect the elastic scattering through virtual couplings. This possible effect was neglected in our $\alpha + \alpha$ phase-shifts analyses that determined the BNP and SPP2 effective interactions. Thus, there is still room for future improvement in these models.

5. The BNP and SPP version 2

Before discussing the new model for the densities, we comment on a minor point that has also been changed in relation to the first

version of the SPP. In the present work, we assume a more current model for the intrinsic charge density of the proton (according to [17]) that again is associated with the intrinsic matter density of the nucleon. Although this new model does not provide significant differences in the results of the nuclear potential, we consider an update of this aspect of the model to be appropriate.

The REGINA code involves the distribution.dat file, that contains information about the theoretical proton and neutron distributions for 11 149 nuclei, ranging from $Z = 2$ and $A = 4$ to $Z = 120$ and $A = 410$. We obtained these theoretical results using the DHB model [3], as described in the next section. The REGINA code calculates the corresponding charge and matter densities defined according to Eqs. (3) and (4).

As already commented, we associate the intrinsic matter density of a nucleon with the charge density of a proton. Therefore, it is also possible to associate the charge density of a certain nucleus to the partial contribution of the protons to the matter density of this nucleus. Since charge densities can be extracted from electron scattering experiments, we can relate this information to the "experimental" determination of matter densities. For instance, for nuclei with $Z = N$, the corresponding matter density is approximately given by twice the respective charge one. As another example, the proton and neutron contributions to the matter density of ^{3}H are related to the ^{3}H and ^{3}He (mirror nucleus) charge densities, respectively. Thus, the (total) matter density of ^{3}H is equal to the sum of the ^{3}H and ^{3}He charge densities. This kind of association allows the determination of "experimental" matter densities through information obtained for charge densities in electron scattering experiments. The REGINA code involves the density.dat file, that contains "experimental" matter and charge densities for some nuclei, including several, such as the deuteron and triton, for which no theoretical distributions are found in the distribution.dat file. The code has an option to use theoretical or experimental densities in the calculations.

The SPP2 and BNP are calculated according to Eq. (7), using the respective effective nuclear interactions (20) and (18). The BNP potential is energy independent, and the SPP2 presents an energy dependence related to the relative velocity between the nuclei. The reader should pay attention to this detail.

6. The theoretical nuclear distributions

The theoretical proton and neutron distributions were calculated using an axially-symmetric self-consistent DHB mean field approximation to the nuclear ground-state [3]. The mean field calculations were performed by iterating an expansion of the wave functions and mean fields in a Gaussian basis to convergence. A Gaussian basis of 16 major fermion shells was used. For each nucleus, calculations were performed for a spherical basis, an oblate basis with $\beta = -0.1$ and a prolate basis with $\beta = 0.1$. The calculation furnishing the lowest energy was taken to be the ground-state. Note that the basis deformation does not determine the nuclear deformation. A nonzero basis deformation merely "breaks" the spherical symmetry, increasing the chances of the code converging to a lower energy deformed solution, when such a solution exists.

Calculations were performed for three Dirac-Hartree parameter sets found to furnish a relatively good description of the ground-state masses and charge radii of near-stability nuclei throughout the entire mass table [18]. These are the DD-ME2 [19], NL3* [20] and NLRA1 [21] parameters sets. An effective finite-range extension of the relativistic pairing interaction of Ref. [3] was used to describe the pairing. Calculations were performed for nuclear charges from $Z = 2$ to $Z = 120$ over a large range of mass numbers. Although the range in mass number was increased for many elements during the several iterations of the calculations, no concerted attempt was made to ensure that all nuclei stable to particle emission have been included.

Table 1
The table presents deviations in binding energy, $\langle \Delta E_b \rangle$ in MeV, root-mean-square deviations in binding energy, $\sqrt{\langle \Delta E_b^2 \rangle}$ in MeV, average deviations in charge radius, $\langle \Delta r_c \rangle$ in fm, and the root-mean-square deviations in charge radius, $\sqrt{\langle \Delta r_c^2 \rangle}$ in fm. The calculation were performed for three different parametrizations of the interaction. The table also provides the number of nuclei included in each group for each set.

DD-ME2						
Nuclei	N_E	$\langle \Delta E_b \rangle$	$\sqrt{\langle \Delta E_b^2 \rangle}$	N_r	$\langle \Delta r_c \rangle$	$\sqrt{\langle \Delta r_c^2 \rangle}$
Light	987	-0.42	2.31	280	-0.012	0.050
Medium	1679	-0.53	1.61	560	0.011	0.032
Heavy	746	-0.66	2.29	109	0.010	0.029
All	3412	-0.53	1.99	949	0.004	0.038
NL3*						
Nuclei	N_E	$\langle \Delta E_b \rangle$	$\sqrt{\langle \Delta E_b^2 \rangle}$	N_r	$\langle \Delta r_c \rangle$	$\sqrt{\langle \Delta r_c^2 \rangle}$
Light	987	0.27	2.95	280	-0.028	0.046
Medium	1679	-0.37	2.92	560	0.007	0.037
Heavy	746	-4.12	5.69	109	0.011	0.028
All	3412	-1.01	3.71	949	-0.003	0.039
NLRA1						
Nuclei	N_E	$\langle \Delta E_b \rangle$	$\sqrt{\langle \Delta E_b^2 \rangle}$	N_r	$\langle \Delta r_c \rangle$	$\sqrt{\langle \Delta r_c^2 \rangle}$
Light	987	0.66	3.42	280	-0.019	0.036
Medium	1679	2.04	2.82	560	0.015	0.031
Heavy	746	1.53	3.47	109	0.019	0.028
All	3412	1.53	3.15	949	0.005	0.032

To compare the three parametrizations, the calculations were separated into three groups: light nuclei, with charge number $Z \leq 20$, medium mass nuclei, with $20 < Z \leq 82$, and heavy nuclei with $Z > 82$. The calculations were compared to experimental binding energies in the 2016 mass table [22] and to the experimental charge radii in Ref. [23], in the cases in which these data exist. For each group we obtained the average deviation in binding energy,

$$\langle \Delta E_b \rangle = \left\langle E_{b,cal}(Z,A) - E_{b,exp}(Z,A) \right\rangle_{Z,A\,\in\,\text{group}}, \tag{21}$$

the root-mean-square deviation in binding energy,

$$\sqrt{\langle \Delta E_b^2 \rangle} = \sqrt{\left\langle \left[E_{b,cal}(Z,A) - E_{b,exp}(Z,A) \right]^2 \right\rangle_{Z,A\,\in\,\text{group}}}, \tag{22}$$

the average deviation in charge radius,

$$\langle \Delta r_c \rangle = \left\langle r_{c,cal}(Z,A) - r_{c,exp}(Z,A) \right\rangle_{Z,A\,\in\,\text{group}}, \tag{23}$$

and the root-mean-square deviation in charge radius,

$$\sqrt{\langle \Delta r_c^2 \rangle} = \sqrt{\left\langle \left[r_{c,cal}(Z,A) - r_{c,exp}(Z,A) \right]^2 \right\rangle_{Z,A\,\in\,\text{group}}}. \tag{24}$$

The values of these deviations for each group and each parameter set are given in Table 1. The number of nuclei included in each group for each set is also given in the table. As can be seen from the values in the table, it is not a trivial task to choose one parameter set as more consistent with the data than the others.

In Fig. 1, we compare the charge radii calculated for the three parameter sets with the experimental data for neon isotopes. We observe that the NL3* and NLRA1 values follow the variations in the experimental data fairly well, while the DD-ME2 calculations only reproduce its average tendency. The variations in the NL3* and NLRA1 calculations are due to variations in the ground-state deformation. Both yield highly prolate solutions for the region around $A = 20$ and for $A > 30$. The NL3* ground-states for $A =$

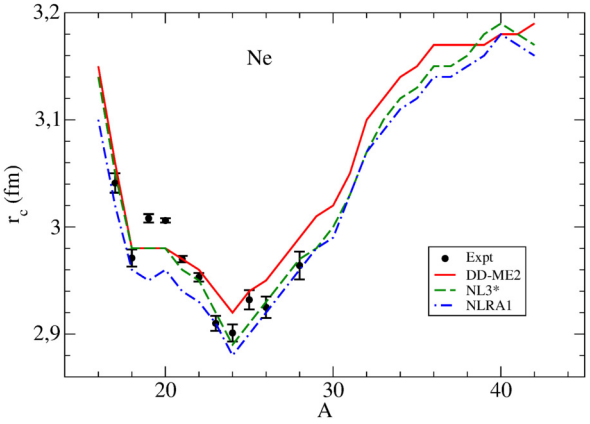

Fig. 1. Calculated charge radii of the neon isotopes for three parameter sets are compared to the experimental ones of Ref. [23].

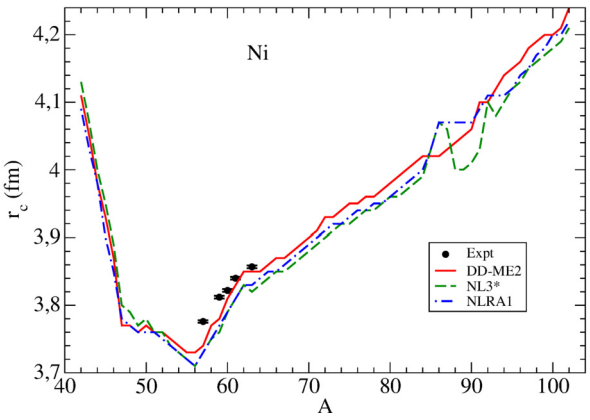

Fig. 2. Calculated charge radii of the nickel isotopes for three parameter sets are compared to the experimental ones of Ref. [23].

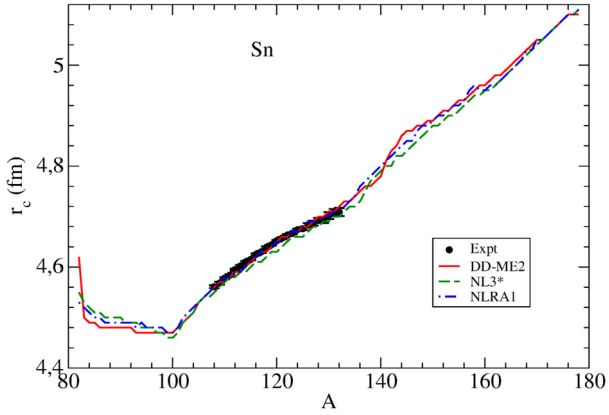

Fig. 3. Calculated charge radii of the tin isotopes for three parameter sets are compared to the experimental ones of Ref. [23].

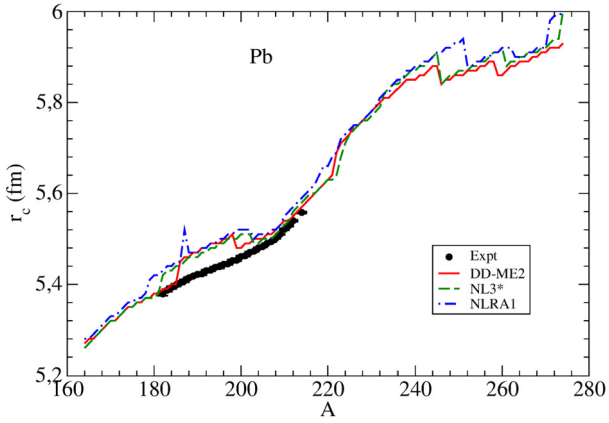

Fig. 4. Calculated charge radii of the lead isotopes for three parameter sets are compared to the experimental ones of Ref. [23].

25, 26 are spherical, which results in a smaller charge radius. The DD-ME2 solutions are uniformly spherical in this case. It must be said that this can not be taken as a defect of the DD-ME2 parameter set, as the deformation involves a delicate balance between pairing and the quadrupole force. The pairing interaction, used in all calculations, seems to have overpowered the quadrupole force in this special case.

In Fig. 2, we compare the charge radii calculated for the three parameter sets with the experimental data for nickel isotopes. The calculations are all uniformly lower than the experimental values by about 0.05 fm. The calculations are quite consistent with one another except at large neutron excess where differences in deformation introduce variations in the effective charge radius. The peak in the NL3* calculation at $A = 86$, in particular, displays the effect on the charge radius of an oblate deformation of $\beta_2 = -0.254$ when compared to the spherical solutions of neighboring isotopes.

In Fig. 3, we show the experimental and theoretical results for tin isotopes. Here we see good agreement between the calculations and the data in the range in which the data exist. At mass numbers above $A = 132$, variations between the calculations begin to appear, mostly due to variations in ground-state deformations of the solutions. The large value of the charge radius of ^{82}Sn for the DD-ME2 parametrization is due to a prolate deformation of $\beta_2 = 0.284$, with the subsequent isotopes being spherical.

In Fig. 4, we show results for lead isotopes. Here we clearly see the effect of ground-state deformations in the deviations of the calculations from most of the experimental data. If the lowest energy solutions of our calculations were the spherical ones, they would have followed the data closely, as do the DD-ME2 calculations below $A = 186$ and above $A = 198$. The DD-ME2 solutions between these two limits are oblate. In contrast, the NL3* and NLRA1 solutions are prolate in the region from $A = 182$ to $A = 202$. The difference in deformation is surprising and will require further study on our part to be understood. However, to agree with the data, the ground-state solutions should be spherical. This is a clear case in which the pairing interaction must be stronger than it is in the calculations. Large variations in the radius are also seen at high neutron excess, again due to variations in the deformation.

After analyzing the average deviations in the binding energy and the charge radius given in the tables and examining figures comparing calculated and experimental charge radii for many isotopic chains, we have chosen to use the DD-ME2 nucleon densities as the basis for the potentials. Although the NLRA1 parameter set approximates the charge radii slightly better, on the average, the DD-ME2 parameter set furnishes a much better approximation to the binding energy. The smoother (on average) isotopic dependence of the charge radius for the DD-ME2 parameter set also influenced our decision. Although the large fluctuations in the charge radius seen, for example, in the region of $A = 86$-94 for the Ni isotopes, as well as in other chains, may one day be proven to be correct, we prefer to adopt the generally smoother DD-ME2 results.

7. The deformation parameters

In the intrinsic frame of reference, the theoretical DHB proton and neutron distributions have axial symmetry and can be written

as a function of the radius r and the azimuthal angle relative to the symmetry axis θ,

$$\rho_t\left(\vec{r}\right) = \rho_t\left(r,\theta\right), \qquad t = p,\, n. \tag{25}$$

In the laboratory frame, the spherical distributions are obtained through the average,

$$\rho_{t,\mathrm{sph}}\left(r\right) = \frac{1}{4\pi}\int \rho_t\left(r,\theta\right) d\Omega. \tag{26}$$

These spherical proton and neutron distributions are used to obtain the folding potentials.

We have used several approaches to extract information on the deformation of the distributions. In the first of these, we use an electromagnetic-type multipole moment to calculate a deformation parameter $\beta_{t\lambda}$ through the approximation

$$\begin{aligned} Q_{t\lambda} &= \int r^{\lambda} Y_{\lambda 0}\left(\theta,\phi\right)\rho_t\left(r,\theta\right) d^3r \\ &\approx \frac{\rho_{t0}}{\lambda+3}\int Y_{\lambda 0}\left(\theta,\phi\right)\left[R_t\left(\theta\right)\right]^{\lambda+3} d\Omega \\ &\approx \frac{3}{4\pi} A_t R_{t0}^{\lambda}\beta_{t\lambda} \qquad \lambda = 2,4, \end{aligned} \tag{27}$$

where we have approximated the integral using a sharp-cutoff density of radius

$$R_t(\theta) = R_{t0}\left[1+\beta_{t2}Y_{20}\left(\theta,\phi\right)+\beta_{t4}Y_{40}\left(\theta,\phi\right)\right], \tag{28}$$

with

$$A_t = \frac{4\pi}{3}\rho_{t0}R_{t0}^3 = Z \text{ or } N, \tag{29}$$

and truncated the resulting expression to first order in the quadrupole or hexadecapole deformation, β_{t2} and β_{t4}, respectively. In order to obtain the $\beta_{t\lambda}$ values, we assume $R_{t0} = 1.2\,A^{1/3}$ fm in Eq. (27). The second approach emphasizes the coupling through the short-range nuclear interaction. Here, we calculate nuclear deformation lengths by assuming that the charge distribution can be written as

$$\begin{aligned} \rho_t\left(r,\theta\right) = \rho_{t,\mathrm{sph}}\left(r\right) &- \delta_{t2}^{(p)}\frac{d\rho_{t,\mathrm{sph}}}{dr}Y_{20}\left(\theta,\phi\right) \\ &- \delta_{t4}^{(p)}\frac{d\rho_{t,\mathrm{sph}}}{dr}Y_{40}\left(\theta,\phi\right), \end{aligned} \tag{30}$$

where the $Y_{\lambda 0}\left(\theta,\phi\right)$ are spherical harmonics and δ_{t2} and δ_{t4} are the deformation lengths relative to the quadrupole and hexadecapole modes for neutrons and protons. We would then expect to have

$$-\delta_{t\lambda}^{(p)}\frac{d\rho_{t,\mathrm{sph}}}{dr} = \int \rho_t\left(r,\theta\right)Y_{\lambda 0}\left(\theta,\phi\right)d\Omega \equiv \rho_{t\lambda}\left(r\right), \qquad \lambda = 2,4. \tag{31}$$

As the radial dependence of the right and left side of these equations are not identical, we estimate best values for the deformation lengths by minimizing the integrals,

$$\int_0^{\infty}\left(\delta_{t\lambda}^{(p)}\frac{d\rho_{t,\mathrm{sph}}}{dr}+\rho_{t\lambda}\left(r\right)\right)^2 r^2 dr, \qquad \lambda = 2,4. \tag{32}$$

Finally, we also extract parameters corresponding to a deformed Fermi function by fitting the deformed density $\rho_t\left(r,\theta\right)$ directly with the function

$$\rho_{tF}\left(r,\theta\right) = \frac{\rho_{t0}}{1+\exp\left[\frac{r-R_t(\theta)}{a_t}\right]}, \tag{33}$$

where $R_t\left(\theta\right)$ is given in Eq. (28). Here, the radius R_{t0}, diffuseness parameter a_t, quadrupole deformation β_{t2} and hexadecapole deformation β_{t4} are adjustable parameters, but the central density ρ_{t0} is constrained so that the integrated density furnishes the correct proton or neutron number. A fit of a Fermi distribution to the spherically average density $\rho_{t,\mathrm{sph}}\left(r\right)$ is also performed.

The distribution.dat file contains the proton and neutron $\rho_{\mathrm{sph}}(r)$ distributions, as well as the deformation lengths δ_{t2} and δ_{t4} obtained from Eqs. (30) to (32), and the R_{t0}, a_t, ρ_{t0}, β_{t2} and β_{t4} values that best fit the DHB proton, neutron and nucleon deformed distributions through deformed Fermi-functions. The best fit Fermi-function parameters for the spherical distributions are also given.

The values of the deformation parameters, β_{t2} and β_{t4}, obtained from the electromagnetic-type moments and the Fermi-function fits to the deformed densities are quite similar. As the radial form of the densities differs from that of a Fermi function, we do not expect them to be identical. We also find reasonably good agreement between the values of the deformation lengths $\delta_{t\lambda}^{(p)}$ and the values $R_{t0}\beta_{t\lambda}$, which would be obtained, for example, from an expansion of the Fermi fits to the densities.

Although values of the deformation lengths and the best fit values for Fermi distributions are given for protons, neutrons and nucleons, we recommend that the values for nucleons be used with care, as the neutron and proton distributions can be quite different, especially in nuclei far from stability.

Note that the δ_{t2} and δ_{t4} values correspond to the average permanent deformation. They do not contain information about vibration (zero-point motion) of the densities around these average values. Thus, the δ_{p2} and δ_{p4} should not be directly associated to the $BE(2)$ and $BE(4)$ Coulomb amplitudes of excited states, nor to nuclear couplings to these states.

An estimate for the parameter values related to the amplitude of vibrations can be obtained within the hydrodynamical model:

$$\sigma_\lambda = R_0\sqrt{2\lambda+1}\left(\frac{\hbar^2}{4B_\lambda C_\lambda}\right)^{1/4}, \tag{34}$$

$$B_\lambda = \frac{3Am_0}{4\pi\lambda}R_0^2, \tag{35}$$

$$C_\lambda = \frac{(\lambda-1)(\lambda+2)a_s A^{2/3}}{4\pi} - \frac{(\lambda-1)3Z^2e^2}{(2\lambda+1)2\pi R_0}, \tag{36}$$

where m_0 is the mass of the nucleon and $a_s \approx 19$ MeV. With this, the total (permanent deformation + vibrational component) deformation length value can be obtained from:

$$\delta_\lambda \approx \sqrt{\left(\delta_\lambda^{(p)}\right)^2+\sigma_\lambda^2}. \tag{37}$$

In principle, these δ_λ values should be more appropriate to use in coupled-channel calculations. Nevertheless, in Ref. [24] was found that, in the case of the excitation of the first 2^+ state of even-even nuclei, the hydrodynamical σ_2 overestimate the quadrupole vibrational contribution by a factor about 2. Larger discrepancies could be expected for nuclei very far from the stability line. Even so, the REGINA code provides these deformation length values.

8. Numerical calculations

Given a pair of nuclei, the code searches for the corresponding theoretical proton and neutron distributions (distribution.dat file) or charge and matter densities (density.dat file) according to the option defined by the user. The densities are calculated from the distributions (or vice-versa), through the definitions Eqs. (3)

and (4). The Fourier transform method is used to relate the spherical densities with the corresponding transforms. For instance, for charge densities we have:

$$F_c(q) = \frac{4\pi}{q} \int \rho_c(r)\ \sin(qr)\, r\, dr, \tag{38}$$

$$\rho_c(r) = \frac{1}{2\pi^2 r} \int F_c(q)\ \sin(qr)\, q\, dq. \tag{39}$$

Eq. (3) results in the following relation among the respective transforms:

$$F_c(q) = F_p(q) \times F_{c/p}(q). \tag{40}$$

The transformation of proton distributions into charge densities (or vice-versa) is performed numerically making use of Eqs. (38) to (40). A similar procedure is used for matter densities and nucleon distributions.

The double-folding potential is also calculated numerically through the Fourier transform method. For instance, Eq. (7) is equivalent to:

$$V_N(R) = \frac{1}{2\pi^2 R} \int F_{m1}(q)\, F_{m2}(q)\, F_{mm}(q)\ \sin(qR)\, q\, dq, \tag{41}$$

where $F_{m1}(q)$ and $F_{m2}(q)$ represent the transforms of the matter densities of the nuclei, and $F_{mm}(q)$ is the transform of the fundamental nuclear interaction:

$$F_{mm}(q) = \frac{4\pi}{q} \int v_{mm}(r)\ \sin(qr)\, r\, dr. \tag{42}$$

In the case of the SPP2, the nuclear potential depends on the relative velocity through Eqs. (7) and (20), while the velocity depends on the potential according to Eqs. (11) and (12). These equations are solved iteratively (for each R value), considering the first $V_N(R)$ value equal to the folding one (without velocity dependence): $V_N(R) \approx V_F(R)$. Usually, the method converges very quickly. It is possible to demonstrate that a necessary condition to obtain convergence is:

$$\left| \frac{8 V_N(R)}{\mu c^2} \left(1 - \frac{v^2}{c^2}\right)^{3/2} \right| < 1. \tag{43}$$

The code also calculates elastic scattering cross sections by solving a single channel Schrödinger equation, considering the following OP:

$$U_{OP}(R) = V_{\rm real}(R) + i\, W(R), \tag{44}$$

where

$$V_{\rm real}(R) = N_R\, V_N(R), \tag{45}$$

$$W(R) = N_I\, V_{\rm real}(R) - N_{\rm overlap}\ [O(R)]^x - \frac{W_0}{1 + \exp\left(\frac{R - R_{i0}}{a_i}\right)}. \tag{46}$$

$V_N(R)$ can be associated to the SPP2 or BNP, according an option defined by the user. The $O(R)$ term in the imaginary part of the OP corresponds to the overlap of the matter densities of the nuclei:

$$O(R) = \int \rho_{m1}(\vec{r}_1)\, \rho_{m2}(\vec{r}_2)\, \delta(\vec{R} - \vec{r}_1 + \vec{r}_2)\, d\vec{r}_1\, d\vec{r}_2$$
$$= \int \rho_{m1}(\vec{r})\, \rho_{m2}(\vec{r} - \vec{R})\, d\vec{r}. \tag{47}$$

This integral is calculated with the same method as the double-folding potential, since the Fourier transform of the δ function is equal to 1. The user can choose the values of the parameters involved in Eqs. (45) and (46). Note that W_0 and $N_{\rm overlap}$ should be provided in MeV and MeV$\times$fm^{3x}, respectively.

As already mentioned, the original SPP has been used as a standard OP in many applications. We consider that the SPP2 can also be used in standard calculations, as long as the parameter values generally assumed for the SPP are adopted in Eqs. (45) and (46) as well, i.e.: $N_R = 1$, $N_I \approx 0.8$, $W_0 = N_{\rm overlap} = 0$. Only in this restricted sense can the SPP2 be considered a parameter-free model. On the other hand, the complete set of parameters involved in these equations allows the user to test other models in eventual data fits. In particular, the shape of the imaginary part of the OP that simulates the fusion process might be related in some way to the overlapping of the matter densities, without necessarily being directly proportional to it. The term $N_{\rm overlap}\ [O(R)]^x$ allows the user to test this hypothesis.

The Schrödinger differential equation is integrated using the Cowell method [4,5]. The code also uses several standard subroutines to calculate Legendre Polynomials, Coulomb Functions, etc.

Care must be taken when calculating elastic scattering cross sections for the particular case of systems involving identical nuclei. In this case, the elastic scattering cross section depends on the spin of the nucleus, which is not provided in our data files. Thus, the user should calculate the cross section by assuming a spin value and adopting the procedure described below (see e.g. [25]).

For identical nuclei, the elastic scattering cross section is given by:

$$\frac{d\sigma}{d\Omega}_{\rm El.}(\theta) = W_e\, \sigma_e(\theta) + W_o\, \sigma_o(\theta), \tag{48}$$

where

$$W_e = \frac{s+1}{2s+1}\ ;\ W_o = \frac{s}{2s+1} \qquad \text{if } s \text{ is an integer,}$$
$$W_e = \frac{s}{2s+1}\ ;\ W_o = \frac{s+1}{2s+1} \qquad \text{if } s \text{ is half-integer.} \tag{49}$$

The REGINA code provides $\sigma_e(\theta)$ and $\sigma_o(\theta)$ and the user can calculate the elastic scattering cross section through (48). The code also provides the reaction cross section (related to the absorption due to the imaginary part of the OP). Again care must be taken in the case of identical nuclei, where the reaction cross section is given by:

$$\sigma_R = W_e\, \sigma_{Re} + W_o\, \sigma_{Ro}, \tag{50}$$

9. Input and output

The code was developed using FORTRAN 77 with double-precision. If no problems occur, the CPU time is very short (a few seconds). The input parameters should be provided in an input file (dados.dat). The density.dat and distribution.dat files should be accessible in the directory. The dados.dat file must provide the following parameters:

AP, ZP, AT, ZT (integer values, AP and/or AT can be negative as commented below)
R_{max}, dR (real values)
E_{cm} (real)
$iopt$, N_R (integer and real)
N_I, $N_{\rm overlap}$, x, W_0, R_{i0}, a_i (all real)
L_{max} (integer)

AP and AT = numbers of nucleons of projectile and target. If positive, theoretical DHB densities from distribution.dat file are

assumed in the calculations, otherwise the code uses the "experimental" densities of density.dat file.

ZP and ZT = numbers of protons of the projectile and target (always positive values).

R_{max} = matching radius for OM calculations (the nuclear interaction should be negligible for $R > R_{max}$).

dR = step-size for the calculation of the potential and integration of the Schrödinger equation.

E_{cm} = Energy in the center of mass frame of reference.

$iopt = 0 \rightarrow$ use of the SPP2 in the OM calculations, otherwise use of the BNP.

N_R, N_I, N_{overlap}, x, W_0, R_{i0}, a_i are parameters values for calculation of the real and imaginary parts of the OP, according to Eqs. (45) and (46).

L_{max} = number of partial waves involved in the OM calculations (the maximum supported value is 2000).

The output file is saida.out. It provides the projectile and target densities and distributions and the corresponding root-mean-square radii.

The code also provides the δ_λ values obtained from Eqs. (30) to (32), the parameters ρ_0, R_0, a and β_λ of the deformed Fermi-functions according to Eqs. (28) and (33), and the ρ_0, R_0 and a parameter values of the spherical Fermi-functions. All these parameter values are given for the proton, neutron and nucleon distributions.

After the densities, the user will find the folded Coulomb and nuclear potentials and the $O(R)$ overlap term. The output also contains the s-wave barrier parameters (radius, height and curvature) considering the real part of the OP, $V_{\text{real}}(R)$, for the nuclear potential. The elastic scattering cross sections are provided in mb/sr and also as a ratio to Rutherford (only for nonidentical nuclei). The code also provides the reaction cross section. In the case of identical nuclei, the user must use Eqs. (48) to (50) to obtain the cross sections.

Declaration of competing interest

The authors declare that they have no known competing financial interests or personal relationships that could have appeared to influence the work reported in this paper.

Acknowledgements

This work was partially supported by Fundação de Amparo à Pesquisa do Estado de São Paulo (FAPESP) Proc. No 2017/05660-0, 2018/09998-8, 2019/07767-1, and Conselho Nacional de Desenvolvimento Científico e Tecnológico (CNPq) Proc. No 304056/2019-7, 302160/2018-3, 306433/2017-6, and project INCT-FNA Proc. No 464898/2014-5.

Appendix A. Supplementary material

Supplementary material related to this article can be found online at https://doi.org/10.1016/j.cpc.2021.108061.

References

[1] L.C. Chamon, L.R. Gasques, B.V. Carlson, Phys. Rev. C 84 (2011) 044607.
[2] L.C. Chamon, L.R. Gasques, B.V. Carlson, Phys. Rev. C 101 (2020) 034603.
[3] B.V. Carlson, D. Hirata, Phys. Rev. C 62 (2000) 054310.
[4] P.H. Cowell, A.C.D. Gormmelin, Appendix to Greenwich Observations for 1909, Edinburg, 1910, p. 84.
[5] M.F. Manning, J. Millman, Phys. Rev. 53 (1939) 673.
[6] L.C. Chamon, B.V. Carlson, L.R. Gasques, D. Pereira, C. De Conti, M.A.G. Alvarez, M.S. Hussein, M.A. Cândido Ribeiro, E.S. Rossi Jr., C.P. Silva, Phys. Rev. C 66 (2002) 014610.
[7] M.A.G. Alvarez, L.C. Chamon, M.S. Hussein, D. Pereira, L.R. Gasques, E.S. Rossi Jr., C.P. Silva, Nucl. Phys. A 723 (2003) 93.
[8] D. Pereira, et al., Phys. Lett. B 710 (2012) 426.
[9] M.A.G. Alvarez, et al., Phys. Rev. C 98 (2018) 024621.
[10] J.J.S. Alves, et al., Nucl. Phys. A 748 (2005) 59.
[11] G.P.A. Nobre, L.C. Chamon, L.R. Gasques, B.V. Carlson, I.J. Thompson, Phys. Rev. C 75 (2007) 044606.
[12] L.R. Gasques, A.V. Afanasjev, E.F. Aguilera, M. Beard, L.C. Chamon, P. Ring, M. Wiescher, D.G. Yakovlev, Phys. Rev. C 72 (2005) 025806.
[13] L.C. Chamon, L.R. Gasques, L.F.M. Alves, V. Guimarães, P. Descouvemont, R.J. deBoer, M. Wiescher, J. Phys. G 41 (2014) 035101.
[14] L.C. Chamon, L.R. Gasques, J. Phys. G 43 (2016) 015107.
[15] L.C. Chamon, L.R. Gasques, J.C. Zamora, J. Phys. G 47 (2020) 005103.
[16] L.C. Chamon, B.V. Carlson, L.R. Gasques, Phys. Rev. C 83 (2011) 034617.
[17] I. Sick, Atoms 6 (2018) 2.
[18] M. Dutra, O. Lourenço, B.V. Carlson, J. Margueron, in preparation.
[19] G.A. Lalazissis, T. Niksić, D. Vretenar, P. Ring, Phys. Rev. C 71 (2005) 024312.
[20] G.A. Lalazissis, S. Karatzikos, R. Fossion, D. Pena Arteaga, A.V. Afanasjev, P. Ring, Phys. Lett. B 671 (2009) 36.
[21] M. Rashdan, Phys. Rev. C 63 (2001) 044303.
[22] Meng Wang, G. Audi, F.G. Kondev, W.J. Huang, S. Naimi, Xing Xu, Chin. Phys. C 41 (2017) 030003.
[23] K. Marinova, I. Angel, At. Data Nucl. Data Tables 99 (69) (2013).
[24] L.C. Chamon, B.V. Carlson, Nucl. Phys. A 846 (2010) 1.
[25] A.S. Davydov, Quantum Mechanics, Addison-Wesley Series in Advanced Physics, Pergamon Press, 1965.